Materials Plus
https://ojs.wiserpub.com/index.php/MP/

Research Article

Characterization of Ti-6Al-4V Bar for Aerospace Fastener Pin Axial Forging

R.P. Turner[1*], C. Smith[1], L. Zneimer[1], L. Medlock[1], A. Simms Ridgeway[1], G.O. Subramanian[1], T. Patel[2], N. Warnken[1]

[1]School of Metallurgy & Materials, University of Birmingham, Birmingham, B15 2TT, United Kingdom
[2]LISI Aerospace, Rugby, CV21 3RQ, United Kingdom
E-mail: r.p.turner@bham.ac.uk

Received: 26 January 2024; **Revised:** 28 February 2024; **Accepted:** 4 March 2024

Abstract: Ti-6Al-4V warm forged fasteners are a critical part of the aerospace industry, as they are used in vast quantities for mechanical joining of components for the fuselage, wing-skin and aero-engine. These components are produced in vast quantities at rapid production rates through multi-blow axial forging However the rate that they are manufactured means that manufacturers rely upon periodic part conformance testing to understand if the part is within tolerance or if any undesirable manufacturing defects such as cracks or underfilling are present. Thus, a right-first-time manufacturing approach is essential to minimize non-conformant scrap. An analysis of the Ti-6Al-4V supplied raw material for axial forging, in a variety of different bar diameter sizes and from different industrial suppliers, was conducted. This was to attempt to understand whether material property variation or operator variation was the root cause for some material behaving differently during the manufacture route. Experimental testing was performed through microstructure characterization and mechanical testing methods. The volume fraction of the β-phase was noted to be marginally higher in material with good forgeability. The hardness of the inner core of the bar appears to be a critical material property for the Ti-6Al4V bar, with an overly hard bar-core hindering forgeability of the bar. This is believed to be due to the hotter central region malleability being key for forgeability. Micro-void porosity was also noted which could lead to stress concentration locations, or crack initiation, and as such is a deleterious property for forgeability. The experienced forgeability of the Ti-6Al-4V bars have been demonstrated to be sensitive to rather small variation in measured microstructure and mechanical property. It is believed that cumulative impacts of small differences, 1% variation in α-phase volume fraction, small variations in elongation to failure, 1% variation in elastic modulus and microhardness profile variation at the center of the bar of less than 10 HV0.3, can combine to significantly impact the forgeability of Ti-6Al-4V bar.

***Keywords*:** alpha phase; beta phase; hardness; microstructure; fractography; tensile; porosity

1. Introduction

The aerospace manufacturing industry is one of the most safety-critical areas of manufacture. Component-size tolerances, materials requirements and component life calculations all take considerable margin of safety in to design and manufacture routes [1] to ensure that components, structures and systems are all safe, compliant with regulations and fit-for-purpose [2]. Fasteners include bolts, screws and rivets, and are used widely across the complex systems involved with aerospace airframe and aeroengine construction, which may require mechanical fastening for strength, rigidity and structural integrity. Aerospace fasteners must exhibit a concomitant range of

DOI: https://doi.org/10.37256/3120244371

desirable mechanical properties, to allow them to have high strength at a range of operating temperatures in-service. However, with sufficient toughness, in the event of component over-load they would be able to plastically deform without experiencing catastrophic failure, and routine ground checks can then identify and replace such fasteners.

Boyer et al [3] considered in depth the materials suitable for fasteners within the airframe and aeroengine sectors, with titanium alloys and nickel superalloys proving highly successful in the applications. Melhelm at al [4] specify the categories of aerospace fastener in detail, including threaded fasteners, blind fasteners and pin fasteners. This work [4] was primarily focused upon aluminum alloys. Although, it is specified in this work [4] that typical fastener loading occurs through either static overload – in tension, bend or shear – or dynamic fatigue caused by cyclical loading conditions, or corrosion. Additional consideration must be given to in-service expected operating temperatures and conditions, for sensible material selection [5].

Further, strength to density ratios should also be considered. In addition to the requirement for very strict safety criteria to be met, the aerospace industry is additionally undergoing a drive to fly more efficiently, with reduced CO_2 and NOx emissions [6]. The easiest way to reduce CO_2 emissions is to reduce overall system mass, in turn leading to fuel savings. In the aerospace industry every kilogram of material saved reduces the annual fuel expenses by US$3000 [7]. Thus, lighter alloys which have mechanical properties fit for purpose are sought. As such, the workhorse aerospace alloy Ti-6Al-4V, commonly used in components including the cooler regions of the aeroengine, the fuselage, the braking systems, is a popular material for aerospace fasteners with a significant range of operating temperature, thanks to its good corrosion resistance, and excellent strength to density [8].

Ti-6Al-4V is an α/β alloy, which can possess differing microstructural features including a fully lamellar structure, a bi-modal structure, and an equiaxed structure. These are obtained in differing volume fractions by varying composition, fabrication, and post-processing treatments. In a drawn wire of the Ti-6Al-4V alloy, the microstructure typically consists of a fully equiaxed microstructure, with intergranular β phase [9]. The α phase in the alloy contributes the high strength of Ti-6Al-4V, however it is also a rather brittle phase. Thus, the β stabilizing vanadium content allows for some retained β phase at room temperature, which offers a greater ductility and toughness, at the expense of some strength and hardness, given that beta is a softer phase than α.

The grain size for the alloy in such a condition typically is 14 to 20 μm, with a texturing occurring due to the wire drawing process elongating grains in the as-drawn direction. There is known significant sensitivity of the mechanical properties of the alloy to the volume fractions of the softer β phase, and the harder α phase, which can be varied with heat treating regimes, however a common estimated value for the beta phase volume fraction is around the 5 % to 7.5 % level, the remainder α [10, 11]. Mechanical properties of the Ti-6Al-4V alloy will clearly depend upon the precise microstructure and phase fractions, however commonly quoted materials properties are an elastic modulus E of 105–115 GPa, an elastic yield strength σ_Y of 950 to 970 MPa, an ultimate tensile strength σ_{UTS} of 1010 to 1050 MPa, and an elongation at break of 19 to 22% [9].

The bar material is manufactured into fastener pin blanks using warm forging methods, whereby specialist axial forging machines continuously heat a constantly unfurling spool of titanium bar using induction heating, as the bar is passed through the induction coil. Subsequently, short pieces of the spooled bar are sectioned into the required size, positioned in a recessed die, and a single or multi-blow forging operation is employed to form the section of bar into a fastener pin blank. As technology develops, machinery to perform these various manufacturing stages has improved such that the commercial machines used in fastener manufacturers can produce upwards of 100 pins per minute. As with any production at this rate, there is clearly no time for operators to visually inspect every single forged part. Thus, successful products require precise processing routes, tight accuracy tolerances, and strategic manufacturing checks to determine conformity of sample parts. Ti-6Al-4V, as all titanium alloys, are highly deformation-rate sensitive materials [12], thus the speed at which the axial forging is occurring, to ensure the machine production rate is a pseudo-production parameter that may get overlooked by manufacturers. However, given the alloy strain-rate sensitivity, forging rate could have significant impact upon the part quality.

The role that the deformation route has upon the deformed part microstructure and properties is considered in the literature. Hu et al [13] were considering deformation and its impact upon microstructure and mechanical property for a novel titanium alloy Ti-5Al-1.5Mo-1.8Fe. They concluded that alloys with bimodal microstructure display improved plasticity capacity than a lamellar microstructure. Zhang et al [14] considered differing forging steps and the role this played in impacting the final material properties. Microhardness was shown to vary from 323 HV to 335 HV, and yield strength from 859 MPa to 907 MPa, based upon the observed microstructural variation.

Whilst Campanella and Fratini [15] performed research work on grade 5 titanium Ti-6Al-4V considered many different manufacturing routes, and forged parts offer an improved consistency in the relative density, higher micro-hardness values than other methods including machining and powder-based additive approaches, whilst

offering only marginally worse buy-to-fly ratios than those associated with power additive routes. Fang et al [16] constructed life prediction models for Ti-6Al-4V forgings based upon input parameter variation. The life variation is again due to small but not insignificant variation in microstructure, giving rise to a variation in material properties.

Finite element methods (FEM) have been employed to study the behavior and deformation of titanium alloys during warm and hot forging [17, 18]. In these works, authors use software including ABAQUS, Deform and Q-Form to predict forging behavior and thermo-mechanical trends. Authors comment that digitalization of predictive capability, the so-called digital twin approach, appears to be the industrially preferred method, largely due to their capability to predict difficult to measure properties, plus the assurance that there is no reduction of production rates caused by experimental instrumentation or data logging.

Due to the very fast production rates, quality assessment on parts can only be performed periodically, on representative small batches of parts. Thus, any non-conformity or defects detected within the forged pins checked may be critical to a considerable number of processed blank pins. Fastener pins and mating holes are researched for their susceptibility to produce defect cracks during manufacture, which can in turn serve as an initiation site for catastrophic crack propagation during cyclic loading or typical in-service loads [19]. Thus, there is considerable pressure on machine operators, and on the manufacturers, to achieve a low scrap rate, and thus ensuring a right-first-time manufacturing capability is met.

As such, the novel approach considered within the present work was intended to investigate to a much more detailed level the relevant materials properties of supplied raw Ti-6Al-4V material bar. Characterization experiments were performed to attempt to understand whether there is any evidence for a variation in bar materials properties being the root cause for an industrially observed difference in material behavior during axial forging, the so-called forgeability of the material. There was no neat relationship regarding good and poor forgeable samples being from one particular supplier, nor was there a relationship with about one bar size being more forgeable than another size. Industrial forging processes are standardized; however, operator set-up can slightly vary. In order to make the work as industrially applicable as possible, a number of samples of the Ti-6Al-4V bar arising from different suppliers, and with different bar diameter, were investigated. Hence, supplied sample material were cut from large coils of industrially used bar, which had been attempted to be axially forged into aerospace fastener pins by a world-leading manufacturer, with significantly differing through-process behavior, were examined for their microstructural and mechanical properties.

2. Materials and methods

2.1 *Ti-6Al-4V alloy*

The chemical composition of the Ti-6Al-4V alloy bar, from provided mill certificates, is quoted in Table 1. However, mill certificates are provided for entire spools of coiled bar, thus their representative nature for specific sectioning of bar are unknown, thus are investigated. Different aerospace fastener designs require different initial diameter of bar-stock; hence a range of differing bar diameters are considered. In order to assess causality for poor material behavior during thermo-mechanical axial forging, the raw material from a selection of high quality and unsatisfactory pin batches was analyzed for its microstructure and mechanical properties. The coiled bar stock was received at the company in standard forms from a number of different suppliers, with a quoted microstructure type of equiaxed alpha-beta, a measured beta-transus temperature of 983–986 ºC. Material had undergone an annealing heat treatment at 780–790 ºC for 1 hour followed by furnace cooling over a period of up to 6 hours, was free of alpha-case, and met all mechanical performance and strength requirements as specified. It is assumed that all other processing (such as homogenizing) at the suppliers prior to issuing to the forging company are similar. However, as with any mill certificates, how precisely the tested quantity of material and measured properties represents the many meters of coiled bar within a supplied coil is unknown. Table 1 summarizes the raw material analyzed, with an explanation of the forging behavior. Most of the raw material forged successfully, however a number of issues presented, in the form of a tendency to crack at the fastener head formation, see Fig 1.

2.2 *Preparation & experiment*

All bar samples were sectioned in to 10mm length, mounted in bakelite, and their cross-sections studied. Increasing SiC grinding paper grit of 120, 240, 400, 800 and 1200 grade were used sequentially, for 2 minutes each. Followed by a MD-Largo abrasive cloth with a 9 µm diamond suspension as a lubricant, followed by MD-Chem polishing cloth using OP-S Colloidal Silica suspension to produce a consistent, planar mirror finish.

Following the polishing, the samples were cleaned for 3 minutes in an ultrasonic bath and then air-dried. A JEOL 7000F SEM was used to study the microstructure and elemental mapping at locations ranging from the center of the bar to the outer diameter, for the samples analyzed. Image-J software was then used to analyze the observed microstructure images, for their phase fraction, β-lath width, and micro-void size and fraction.

A Wilson VH1202 Vickers microhardness test was undertaken following ASTM standard E92-17, on the bar cross-section, at positions along the radius of the bar. An indent load of 300 g (HV 0.3) and a dwell time of 10 seconds was used for each indent. A spacing of 0.45mm was implemented in the radial direction. Parallel sets of readings were taken to confirm the repeatability of the measurements. The Diamet software measured the horizontal and vertical axis of the diamond indentations allowing the Vickers hardness to be determined. A Zwick Roell ZMART Pro using serrated tooth grips was used for tensile testing, in accordance with BS EN ISO 6892.1. Bar lengths of 150mm were placed such that the gauge length, measured via an extensometer, was 100 mm in length. Starting crosshead speed for determining proof stress was 2.25 mm/min, whilst the final crosshead speed for determining ultimate tensile stress (UTS) and elongation to failure was 18 mm/min.

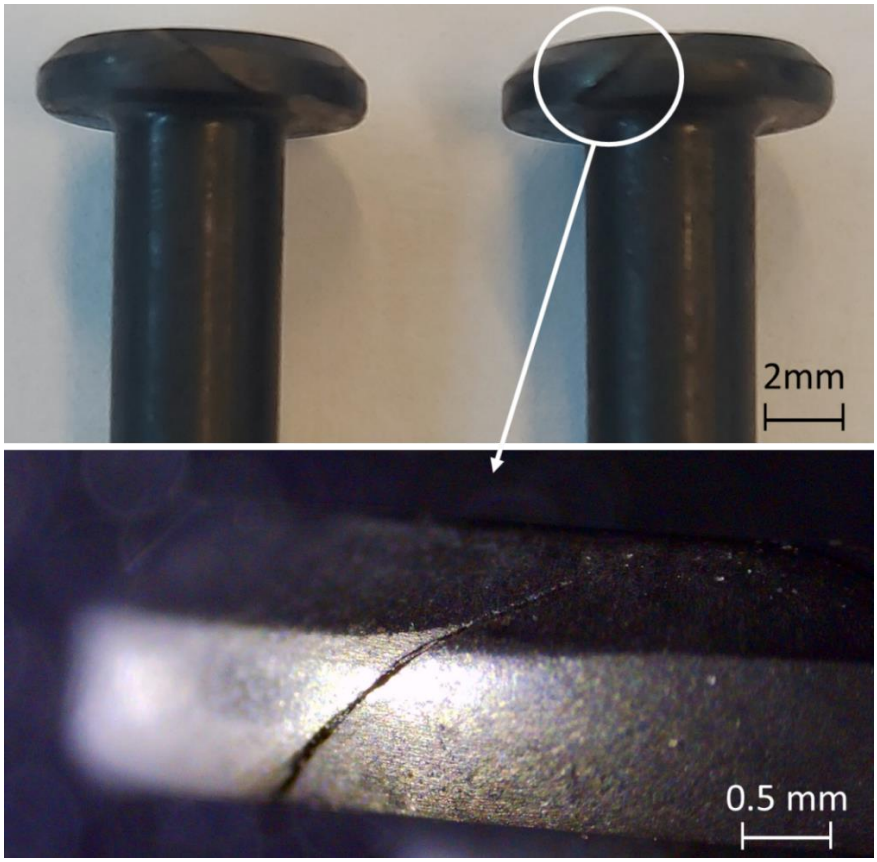

Figure 1. Cracked heads during warm forging manufacturing of the fastener

Table 1. Bar diameter and forging behavior

Sample	Bar diameter (mm)	Composition (wt%)						Mechanical property		Observed forging behavior
		Al	V	Fe	C	O	Ti	σ_{UTS} (MPa)	$\sigma_{0.2\%}$ (MPa)	
1	6.1	6.4	3.9	0.18	0.022	0.15	Bal.	1118	967	Good - Successfully axially forged into pins
2	7.7	6.2	3.85	0.17	0.019	0.15	Bal.	1114	960	Good - Successfully axially forged into pins
3	4.6	6.3	3.95	0.19	0.018	0.15	Bal.	1108	958	Good - Successfully axially forged into pins
4	6.1	6.4	3.9	0.18	0.022	0.15	Bal.	1118	967	Poor - Difficult to forge – tendency to crack

5	6.1	6.4	3.9	0.18	0.022	0.15	Bal.	1118	967	Poor - Material overly hard when forging
6	6.1	6.4	3.9	0.18	0.022	0.15	Bal.	1118	967	Poor - Difficult to forge – tendency to crack

3. Results

After the experimental preparation work, the SEM images were gathered, followed by the hardness testing upon the same planar mirror finish samples. In parallel, the two 150mm bar lengths from each raw material were tensile tested. The results for each experimental procedure are presented in turn.

3.1 *Microstructure characterization*

SEM analysis was performed in backscattered electron (BSE) imaging, as that the BSE detector can better identify the α and β phases with different compositions. Three to five images per sample location were considered when constructing phase volume fraction estimates, with all six bars examined at representative cross-sections. Microstructure analysis was performed for the raw, unforged material. Samples from bar-stock with good forgeability and from bar-stock with poor forgeability, at regions close to the axial center of the round bar, and regions close to the outer diameter edge of the round bar. Representative BSE images for sample 1 – a good forgeability material, can be seen in Figure 2. There was minimal variation in specimen microstructure for different locations within the cross-section, thus alpha grains maintained a uniform size, beta laths were also of a generally uniform thickness, when taking in to account the experimental error associated. Porous voids were marginally larger at the outer radius than the center, likely a consequence of the bar-stock manufacturing route prior to being received at the pin manufacturers.

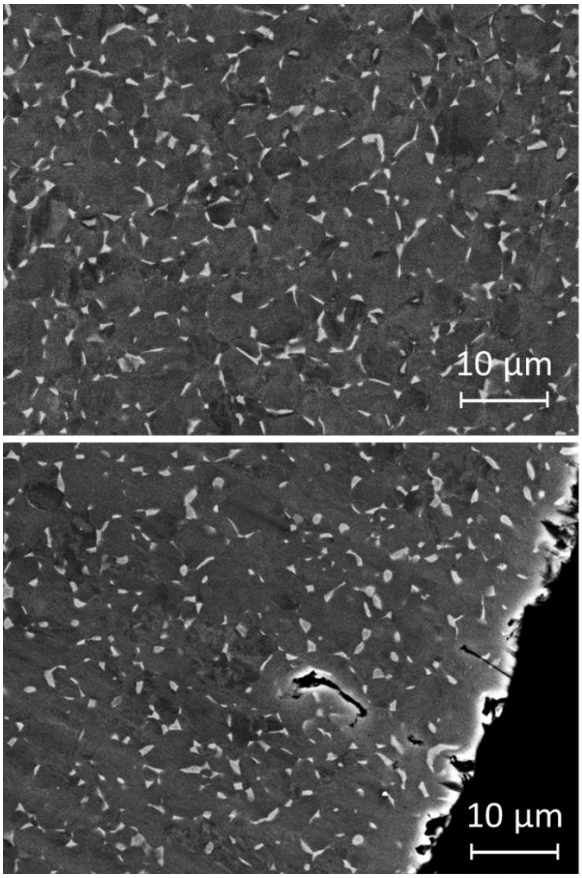

Figure 2. Backscattered Electron (BSE) SEM imaging for central and edge regions in Sample 1

The α-phase is shown in the darker grey coloration in BSE images, whereas the β-phase is shown as the lighter regions. The use of the EDS detector integrated into the Mira TESCAN scanning electron microscope

allows for the chemical composition of the alloy at different locations to be examined and compared. Targeted chemical analysis of a point location in the large α phase grains, and in the β phase lamellae was identified through energy dispersive spectroscopy (EDS) analysis. This is presented in Figure 3, with the corresponding EDS spectra, and was undertaken to understand if any significant chemical variance was observed between well behaved and poor forgeability raw material. The resulting compositional data of the major metallic elements detected are presented in Table 2.

As is understood from fundamental titanium metallurgy [20], Al is an α-phase strengthening and stabilizing addition, whilst V and Fe are β-phase stabilizers. As such, it is as expected to see the V and Fe chemical wt% so much higher in the β laths than their baseline composition, whilst the Al is depleted in the β. Similarly, the Al composition is greatest in the α-phase, whilst Fe and V are depleted. However, there is very little statistically significant variation between the good forgeability samples and the poor forgeability samples in their chemistry. What has not been considered in this table is the presence of lighter elements, such as Oxygen, which is a known strong α-phase stabilizer.

Table 2. Measured elemental composition, in both α-phase and β- phase, and in both well forged raw material and poorly forged raw material

Phase	Element (wt%)	Good forgeability material	Poor forgeability material
α	Ti	88.27 ± 2.82	86.62 ± 2.48
	V	2.96 ± 0.17	3.08 ± 0.17
	Al	5.74 ± 0.21	5.86 ± 0.19
	Fe	0.13 ± 0.09	0.12 ± 0.09
β	Ti	79.09 ± 2.51	80.5 ± 2.36
	V	10.66 ± 0.38	9.48 ± 0.32
	Al	3.8 ± 0.14	4.34 ± 0.16
	Fe	1.65 ± 0.12	1.49 ± 0.1

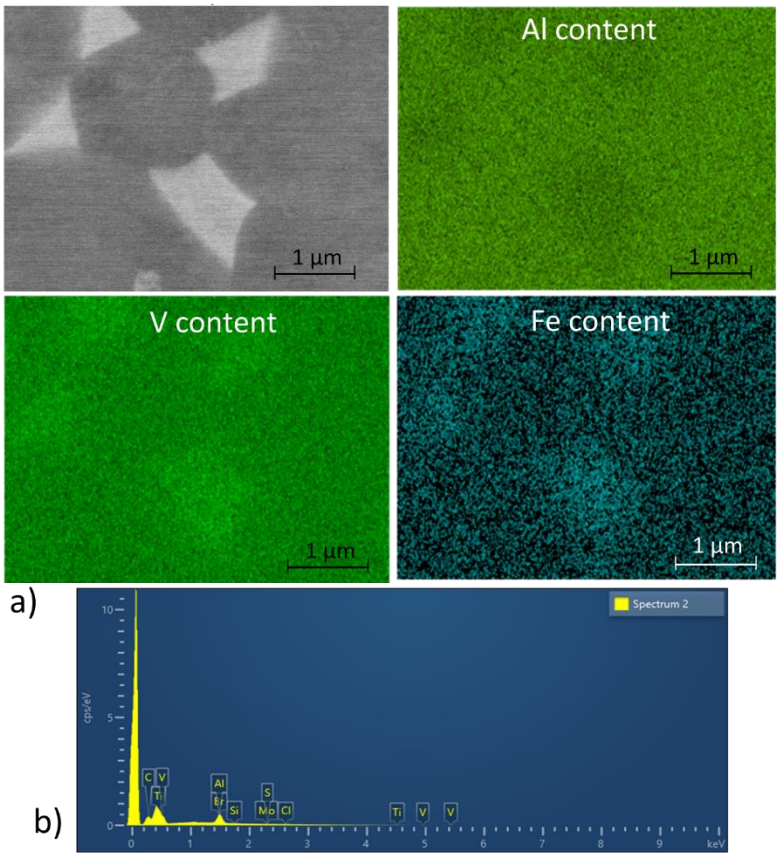

Figure 3. (a) EDS analysis of specific α-phase and β-phase locations in the microstructure, (b) EDS spectra

By further imaging processing using the open-source tool Image-J, estimates for the volume fractions of the α and β phases can be made. Additionally, using the Grain Intercept method, the average size of the room temperature α grains and the β laths are quantified from the BSE images, provided in Table 2. As such, at central and outer radius locations, the α-phase, β-phase, α grain size and β lath sizes are quantified, with appropriate confidence intervals from repeated measurements, in Table 3. Further, the presence of pores (Figure 4) was incorporated into the volume fraction calculation. Thus, the representative weakening caused by the porosity can be quantified. Average pore size for the specimens were also measured, see Table 3.

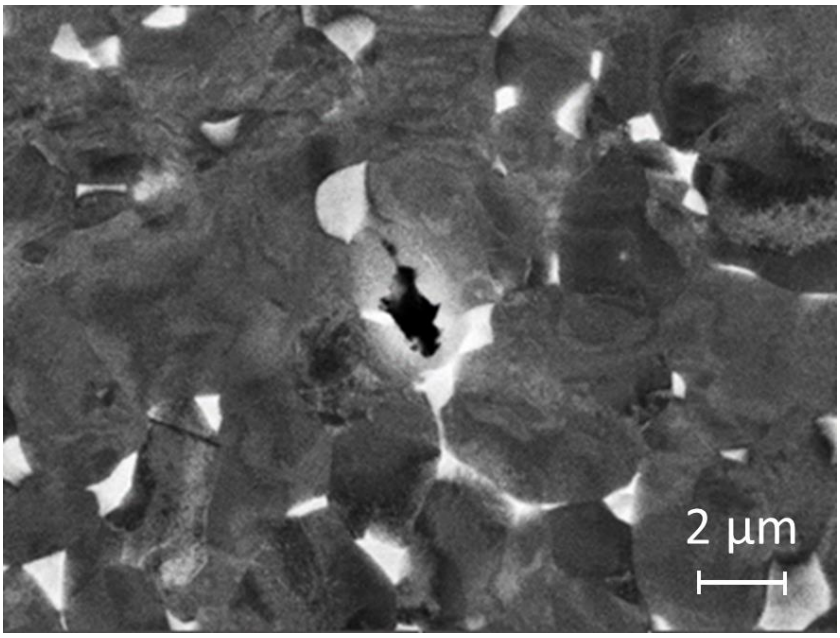

Figure 4. Porous regions detected in Ti-6Al-4V microstructure, indicated by deep black coloration

Table 3. Mean measured volume fractions of α-phase, β-phase and void porosity, at regions close to the center of the bar, and at the outer radius, for good forgeability (bars 1-3) and poor forgeability (bars4-6) material

Location	Phase	Vol. fraction of phase (as %)		feature / pore mean size (µm)	
		Good forgeability material (Bars 1-3)	Poor forgeability material (Bars 4-6)	Good forgeability material (Bars 1-3)	Poor forgeability material (Bars 4-6)
Outer radius of bar	α	94.5 (+/- 1.0)	95.4 (+/- 0.6)	5.5	5.5
	β	5.3 (+/- 0.6)	4.5 (+/-0.2)	0.44	0.36
	Micro-void	0.102 (+/- 0.01)	0.12 (+/- 0.01)	0.13	0.14
Centre of bar	α	93.9 (+/- 1.5)	94.3 (+/- 0.7)	5.5	5.5
	β	6.0 (+/- 0.6)	5.5 (+/- 0.3)	0.43	0.33
	Micro-void	0.100 (+/- 0.01)	0.117 (+/- 0.01)	0.11	0.12

There was no noticeable variation in the α-phase grain size between forgeable and poorly forgeable samples, thus this does not seem to be a factor on material forgeability. However, there is 0.4% to 0.9% higher α-phase fraction in the poor forgeable bar than in bar with good forgeability. Additionally, there was however a general trend for the amount of β-phase volume fraction to be marginally higher in the center than the outer radius, and the reverse true for the α-phase to make up to unity. However, this trend was observed in both forgeable and poor forgeability Ti-6Al-4V, see Figure 5. Albeit the amount of β-phase present overall was higher at all locations measured in material with good forgeability.

Overall, there is a general trend for the raw material with poor forgeability to have marginally lower β-phase volume fraction (roughly 0.5%), which would make sense from a ductility perspective. However, Bar 2 certainly has higher β-phase content and lower α-phase content than poor forgeability bars. Thus, it is hypothesized that the central region of the bar, where a forged pin will remain hottest and therefore most deformable, is the most important location for the ductile β-phase to be in sufficient quantity. There is a trend for the beta phase fraction overall to be higher in the smallest wire diameter Sample 3 (5.7 %), and lower in the larger wire diameter Sample 2 (5.1 %). These samples are both good forgeability raw material, which would suggest that this level of variation

of the β-phase is an acceptable range. Previous studies have shown that the optimum process window of good formability of Ti6Al4V is relatively narrow, higher content of α phase could result in the reduction of ductility whereas higher content of β phase could cause the softening of the material [21].

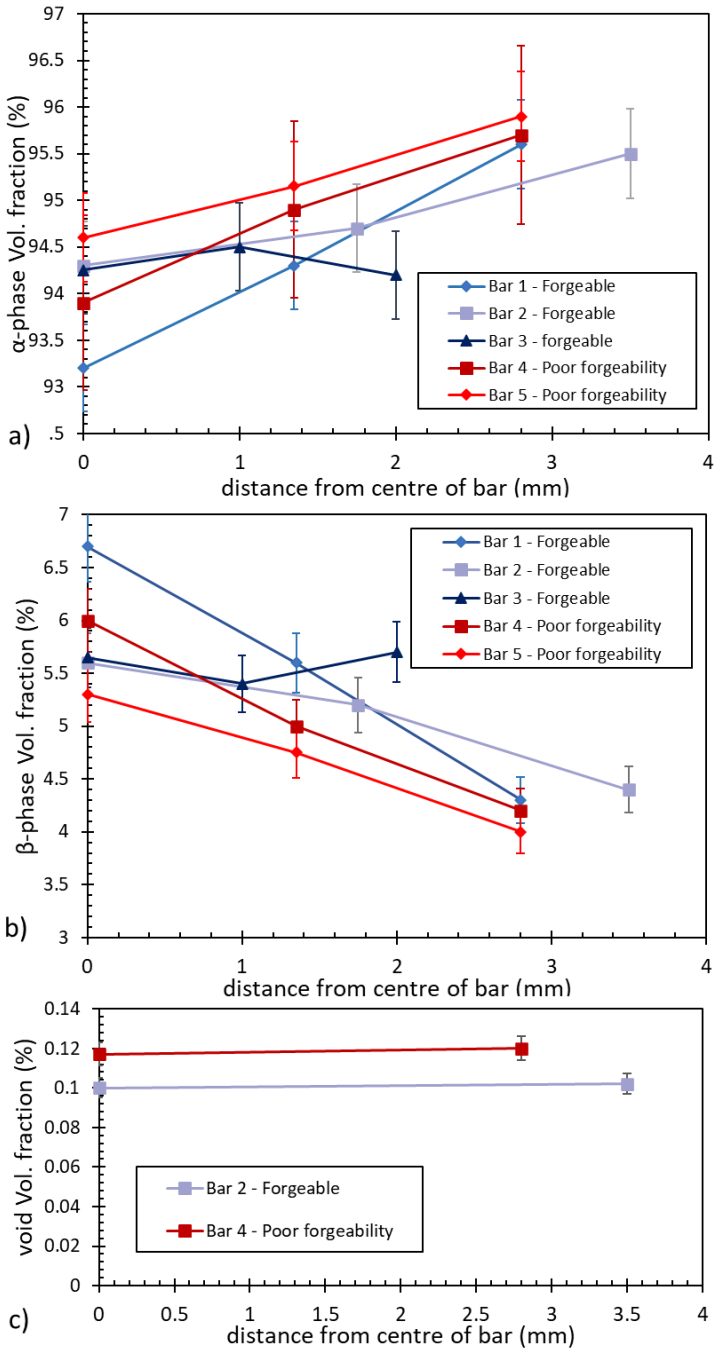

Figure 5. (a) varying α-phase; (b) varying β-phase, (c) varying void Volume fraction, along the radius of the bar cross-section, per bar

The proportion of voids in the measured cross-sectional areas, representing volume fractions of voids, was slightly smaller in bars with good forgeability (0.1%) compared to bar with poor forgeability (0.12%). Porosity tends to be relatively uniform across the diameter of both good and poor forgeable bar. Variation in the α and β phase fractions supports the hypothesis that the poor forgeable material, with a β-phase volume fraction of only 4–4.5% at edge regions, and up to 5.5% at the central region, is too low, promoting overly hard, brittle responses to mechanical loads. It also follows that higher oxygen content, from oxygen pick-up from the atmosphere, will be highest at the outer radius edge of the bar. This promotes greater α-phase stability on the outer edge given that oxygen is a strong α stabilizer, and thus increasing strength and hardness in an α-case type formation.

3.2 *Hardness*

The hardness profiles as obtained by the micro-hardness measurements, for the well-behaved bar material, and the poorly forgeable bar material, are shown in Figure 6. A clear trend is repeatably observed for samples of the well-behaved bar, with the central region being slightly softer than the outside diameter. A gradual increase in hardness is observed moving from center to edge, hardness ranging from 300–312 HV0.3 at the softer center, to 325–330 HV0.3 at the hard outer edge.

These values agree relatively well with those measurements quoted in the literature [22,23] for as-cast Ti-6Al-4V hardness, typically around the 330 to 340 HV0.3 level. Although it is appreciated that precise heat treatments during the initial manufacture are unspecified and could give some variation in the hardness absolute values [24]. This again offers support for the hypothesis that some thin layer of α-case formation at the surface is hardening the bar, and overly constraining the surface. For poor forgeability bar, hardness as a function of the position along the radius varies more, with hardest regions measured away from the edge, or softest regions measured away from the center.

The hardness profiles appear to be very interesting. The very repeatable trend for the bars that did forge successfully into the fasteners, whereby the core of the bar was considerably softer than the harder outer radius region of the bar, follows conventional trends for bar manufacture. The bar that the pins are manufactured from is of a very small diameter, typically 4.5 to 7.5 mm diameter. This would typically mean that the bar manufacturing route would be similar to wire, whereby the bar is produced in considerably larger sections, and is reduced to smaller diameter through drawing operations. Hence, the bar is passed through a series of dies to gradually reduce its diameter by appropriate amounts per stage, with appropriate die angle values [25]. This will impart a residual stress field upon the bar, with the highest compressive stresses occurring in the heavily worked outer diameter of the bar [25]. It could then be inferred that processing parameters of the drawing operation, such as control of workpiece temperature, die temperature, feed speed, may play an important role in the development and magnitudes of the stress field.

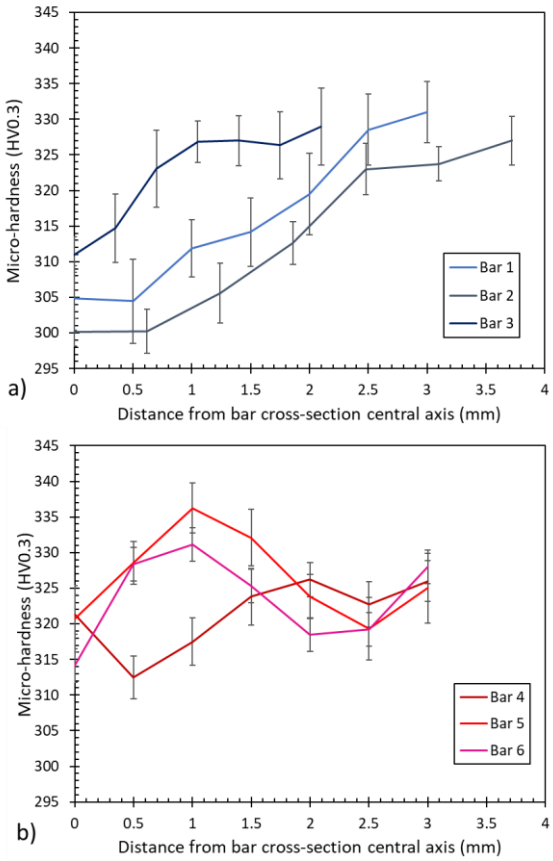

Figure 6. Micro-hardness plots along the bar cross-section radius for (a) forgeable material in Bars 1 to 3, and (b) poor forgeable material in Bars 4 to 6

Further, the diameter of the formed bar may also be important in the local hardness. As the diameter reduces to smaller sizes, it is likely that further stages of drawing were performed, producing greater residual stress at the surface and penetrating deeper into the bar. Figure 7 illustrates how the small diameter bar has higher overall hardness, as the once softer core has now been work-hardened more as the reduction in diameter allows the residual stress to penetrate closer into the center. This may cause the narrower diameter bar to resist deformation even more than larger bar. It is also important to consider that as bar diameter changes, it is likely having an impact upon the required strain and strain rate for the deformed material to fully fill the die recess for the blank pin manufacture. Thus, yet another process variation which is perhaps slightly overlooked by manufacturing engineers, may be impacting upon the through process behavior.

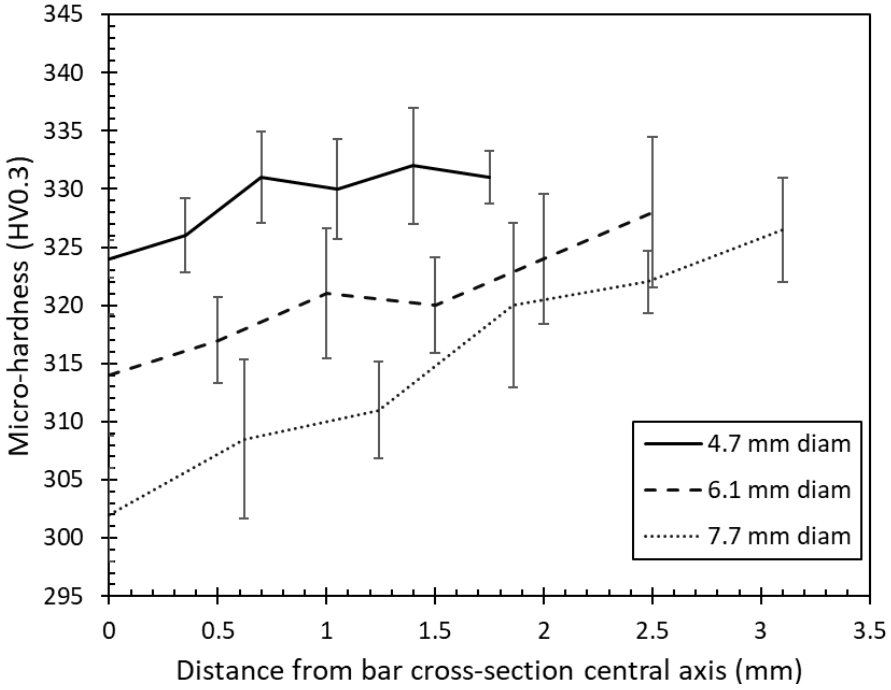

Figure 7. Micro-hardness along the radius of bars for differing bar diameter

3.3 *Tensile Strength*

The resulting stress-strain curves generated by the tensile testing are presented in Figure 8. The tensile curves were relatively consistent with one another, even when comparing the forgeable and the poorly forgeable material. However, if closer inspection of the data is performed, some differences may suggest reasons for the different forgeability of the different supplied alloy.

The premature breaking of the two samples from the supplied bar 3 is likely caused by experimental set-up, with failure occurring closer to the gripped regions of bar, rather than the extensometer measured gauge length. Hence, if these results are somewhat discounted, then the consistency of the necking behavior in tests from bars 1 and 2 is reasonably good. Whereas a more inconsistent necking behavior during elongation to failure is evident in one of the poorly forgeable samples, evident for sample 6, which had a considerable variation of 6.9 % and 8.6 % elongation at rupture during the two tensile tests.

Additionally, the elastic region of the stress strain curves is highly consistent in the samples from material that was of good forgeability, with modulus of elasticity measurements highly repeatable at 99 to 101 GPa. Note that the elastic deformation linear region is fully consistent across all 6 tests. Whereas, for the samples from poor forgeability bar, there is a slightly larger spread in the linear response during the elastic part of the tensile test. This is evidenced by the clustering of the lines being rather less tight, with slightly worse repeatability, giving rise to modulus of elasticity measurements from 95 to 99 GPa. Whilst Young's modulus tends to be marginally higher, by roughly 1–2%, for the bar with good forgeability, at least one of the poor forgeability material has comparable higher modulus. Thus, it is not a definitive trend dividing the forgeable from poor forgeability material.

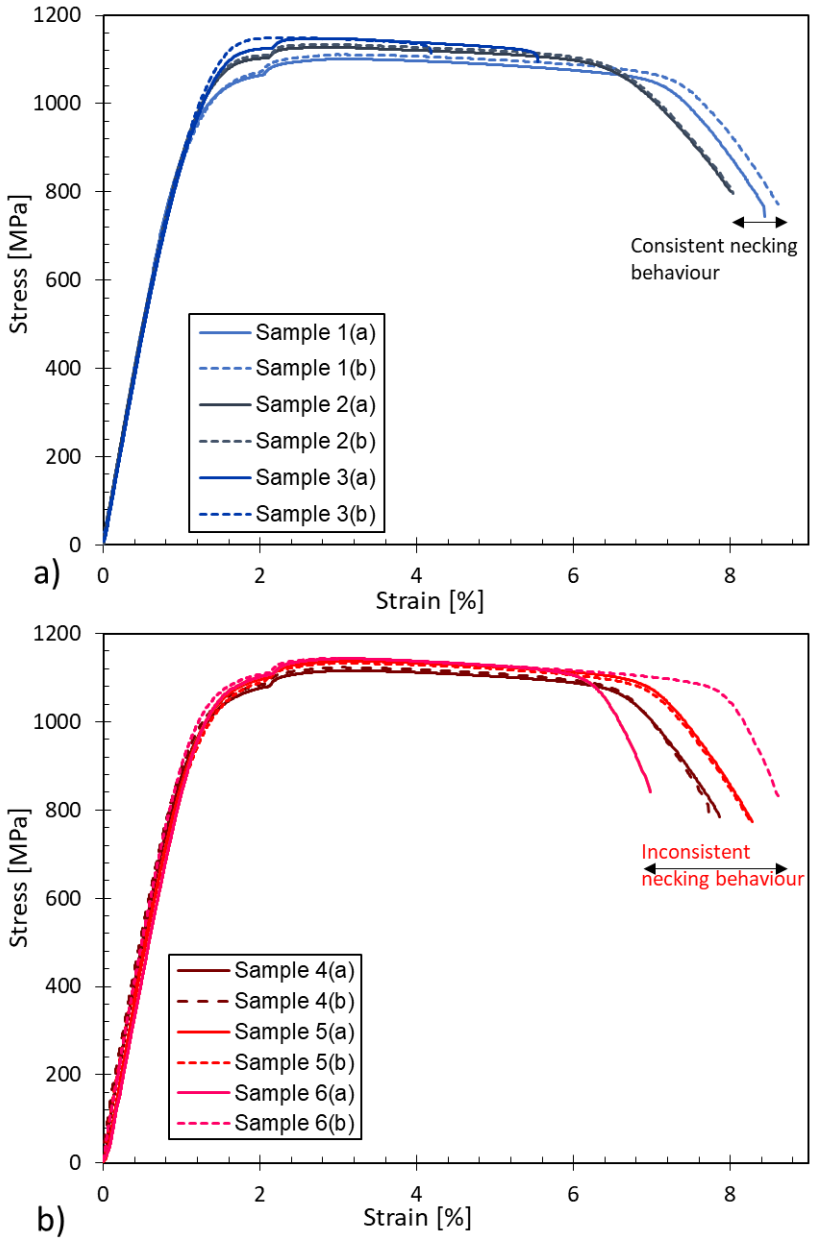

Figure 8. Measured tensile stress – strain curves for representative bar, for (a) good forgeability raw material, and (b) poor forgeability raw material

The yield strength for the raw material showing good forgeability again is relatively consistent, ranging from 948 to 968 MPa. Whilst in the poor forgeability material it is again consistent, albeit marginally lower, at 935 to 951 MPa. However, significant overlap would suggest this is likely not a causation for forgeability differences. The measured elastic and plastic parameters of the stress-strain response are presented in Figure 9. The similarity of the elastic portion of the curves for well-behaved and poor forgeability material would suggest that the bulk mechanical behavior has little bearing upon the ability of these materials to be forged successfully. This perhaps seems to be more sensitive to the plastic deformation and elongation to failure, discussed prior.

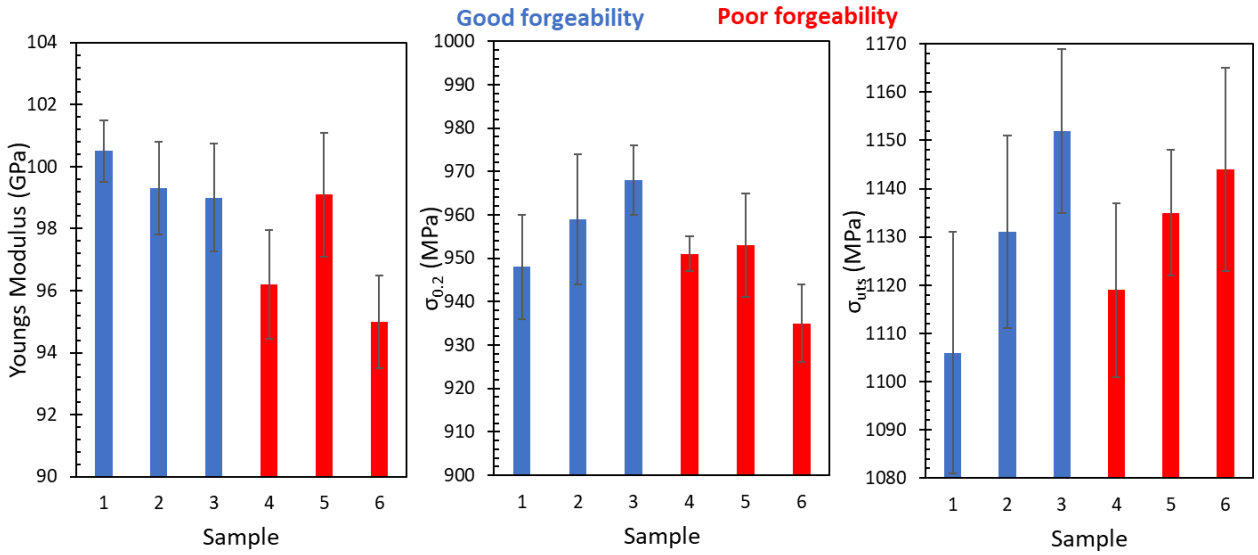

Figure 9. Mean tensile properties of the different bars, a) Elastic modulus, b) 0.2% yield stress, c) ultimate tensile stress, from repeated tensile testing

Fractography of one of the fractured tensile specimens from Bar 2 – with good forgeability, was compared with that of Bar 4 – with poor forgeability. Upon observation, the fracture surfaces presented in Figure 10 shows largely similar, comparable ductile fracture trends between (a) sample 2 and (b) sample 4. The ductile fractures are evidenced with the cup and cone dimpled texture present on the fracture surface, indicated by the dimples highlighted on the microscopy images. For a ductile metallic fracture, micro-voids (indicated by the voids highlighted on the microscopy images) grow, and experience coalescence under severe plastic deformation, which has produced the characteristic ductile fracture surface morphology. The equiaxed dimples present in both forgeable and poor forgeable samples are of similar size and depth, again highlighting the overall similarity of the fracture behavior.

A ductile fracture mechanism in duplex titanium alloy components, such as is evident for both of the bars considered in fractography experiments, must be considered with regard to the more brittle α phase, and the more ductile β phase. Comparing the phase proportion analysis from EDX methods, the marginally larger volume fraction of ductile β phase present in the bar with good forgeability would suggest that this would have more evidence of ductile failure in analyzed fractography. There are more micro-void pores noted in the analyzed forgeable Sample 2 bar, which would suggest higher ductility and a greater elongation to failure in the alloy's stress- strain behavior. However, this observation is based upon a limited number of analyzed fractography surfaces. Additionally, the mechanical testing has not necessarily taken into account the anistotropic behavior [26] of the alloy. As discussed in the tensile testing results, mechanical elastic properties and plasticity behavior of the forgeable and poor forgeability samples was not conclusive, thus it is assumed that any noted fractography variation is not significant for measured mechanical property.

Micro-voids, which can help promote the ductile fracture behavior through void growth and coalescence mechanisms have already been evidenced in microstructure analysis in both good forgeable and poor forgeability material.

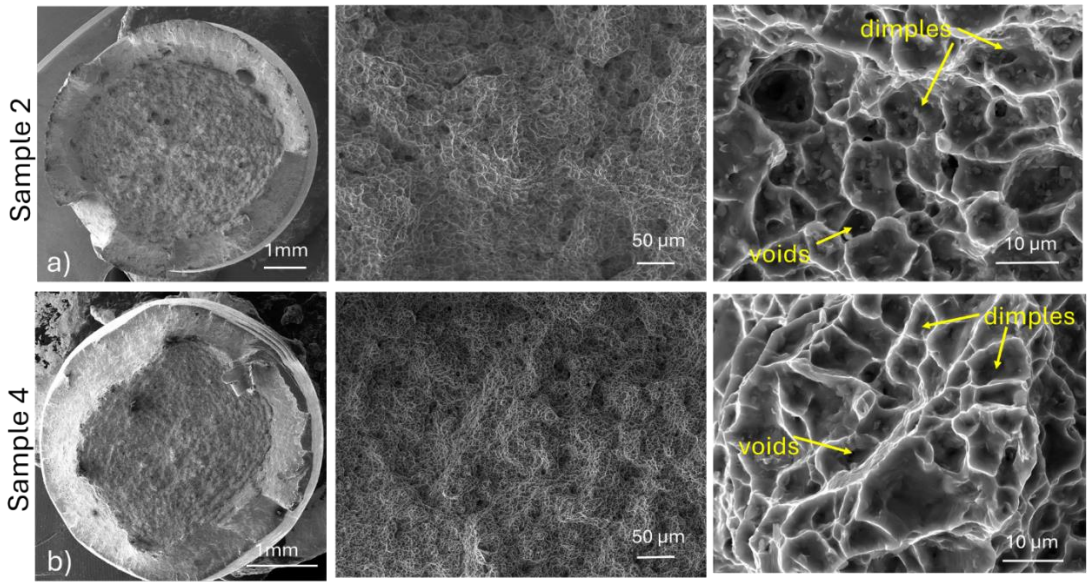

Figure 10. Fractography of the tensile test pieces for (a) sample 2 – forgeable material, and (b) sample 4 – poor forgeability material

4. Discussion

The trends noted in the microstructure, the mechanical properties of the material samples and the fractography often showed only very minor variation between samples with good and poor forgeability. This would suggest that potentially there is no single overarching causation for supplied bar Ti-6Al-4V material to become susceptible to poor forgeability, but rather a cumulative effect caused by several small variations, noted in the measured results for phase fraction, void size and fraction, tensile properties and hardness properties. These potentially combine with geometry factors such as the bar diameter, and the required strain to fill the closed die recess. As such, a deeper consideration of these mechanical properties, voids and phase fraction results is deemed to be necessary for a full assessment of how the forgeability of Ti-6Al-4V bar is determined.

The mechanism for the formation of porous voids in the alloy is unknown, as this would have occurred during the manufacturing route rather than any heating operations as a precursor to axial forging into fastener pins. It is hypothesized that pores could nucleate at the α/β phase boundary during the solidification, due to thermal expansion or flow stress mismatch between the two phases. The β phase is considerably softer than α phase and given the subtle variation of the β phase volume fraction across samples, some material may be more susceptible to void formation during the processing.

Pore formation is a fundamental metallurgical phenomenon which can be difficult to place in either advantageous or deleterious category for the forgeability of a material. It seems intrinsic that the presence of pores will reduce the force required to deform the heated alloy, thus making them more malleable when at the forging temperature. However, it is equally plausible that pore formation can act as; (i) a stress concentrator, raising the residual stresses within the material during plastic deformation and allowing a manufacturing process to reach the material yield stress more readily, and (ii) can act as the nucleation site for further crack propagation. Given that through-process forge cracking is the primary reason for a forged fastener pin to be deemed unsatisfactory, the presence of voids is a key question for further consideration.

Tammas-Williams *et al* [27] looked at the influence of porosity on crack initiation and propagation in titanium alloys manufactured via additive methods, which are known to have potentially high porosity content due to this novel manufacture route. They concluded that the ratio of pore depth from surface, d, to pore diameter, D, was a key contributor in stress concentration effects caused by the porosity. When this ratio was close to 1, and the pore diameter closely matches the depth below surface, the stress concentration is greatest, and can result in a stress concentration K_t term approaching 5. The aspect ratio of the pore also is important, with elongated pores again having a greater impact upon stress concentration. This location of porous voids within the bar may be impacting upon the resulting mechanical behavior within these drawn-bar specimens within this work, as pore distribution was noted to vary slightly between forgeable and poor forgeability samples, and marginal variation for pore fraction with radial location. Notably, a drawn bar manufacturing route is highly likely to elongate any

void defects in the direction of drawing, thus differences in the drawing operation before the fastener pin manufacturer receive the material, may be inherently presenting stress concentrator sites during manufacture.

The hardness profiles measured give rise to some interesting questions that a metallurgist would typically wish to understand. If it is assumed that the hardness is arising as result of the mechanical work upon the bar during manufacturing, then the residual stresses formed, in terms of their magnitude and the locations of regions of high compressive stress, are of importance. Interdependence between the levels of residual stress present and the hardness [28], and the arising impact of hardness upon the flow stress of the material [29] would suggest that relatively small variation along the radius in hardness can cause a stiffening of the material. This could prevent it from shearing as required. This may have an impact upon the material resistance to deform at specified forces. Thus, the increased resistance to deform for the outer section of stressed, harder material could be intrinsically causing issues associated with cracking in the very outer sections of the fastener head formation, where strains are clearly going to be greatest.

If the thermo-mechanical aspect of the process is taken into consideration, these sections of bar will have been heated to approximately uniform operating temperature for warm forging (roughly 500 to 550 ºC) by the continuously fed induction coil. However, as soon as they exit the induction coil and are sectioned and transferred to the forging dies, they begin to cool. It is evident that the cylindrical section will cool fastest on the external edge as heat is lost to the cool atmosphere. Although this rate of heat loss is relatively slow, as the part is only warm forged, so radiative losses are minimal. Recall radiative heat loss follows the Stefan Boltzmann law $W = \varepsilon\sigma(T - T_{atm})^4$ whereby W (W/m^2) is the emitted thermal energy per unit area per second, ε the emissivity of the material, σ the Stefan Boltzmann constant 5.67x10^{-8} W.m^{-2}.K^{-4} and T_{atm} the atmospheric temperature. However, heat will also be lost from the section of bar as it is brought in to contact with the dies for the forging blow, again with the heat being lost at the surface regions of contact with the die.

Hence, (i) the small process variation caused by numerous heat transfer mechanisms causing some heat loss at the surface, coupled with (ii) the role that near-surface voids may play in raising local stress concentration. Additionally, (iii) the likelihood that from the initial bar manufacturing route the outer region is likely to have higher residual stress, and thus higher hardness, thus higher resistance to deformation, and (iv) the varying process strain and strain rates caused by differing initial bar diameter, can influence microstructure and property. These small individual impacts may have cumulative effects which could trigger the defect forming conditions for forging cracking to occur.

It is possible that a heat treatment operation to normalize the microstructure could be applied to all raw Ti-6Al-4V bar stock prior to its use in axial forging. This should reduce process variation between different coils. This type of heat treat operation can however impact upon properties such as hardness profiles through the depth, yield strength and ultimate tensile strength [30]. These properties have been identified in this work as potentially significant in determining the through process behavior, thus a heat treatment application prior to axial forging may influence the forgeability. Additionally, given the considerable number of manufactured axially forged fastener pins from the raw material, and the considerable costs of running heat treatment furnaces for large volumes of material, it seems that this approach would struggle to be justified for adoption into a standard processing route. It is likely that additional manufacture costs would outweigh potential cost saving through scrap reduction. In order to maintain an industrially relevant solution the solution cost must not exceed the scrap costs.

Impact toughness or impact resistance is an important consideration for aerospace applications of structural fasteners [31]. Whilst this has not been considered in this work, due to the sample size required for Charpy type impact toughness measurements compared to the diameter of supplied bar-stock, further experimental work would be proposed for a more comprehensive understanding of the alloy mechanical response, including factors such as Charpy impact testing.

Through-process understanding of material behavior, such as those gained with process modelling finite element methods, can be cost-effective ways to analyze manufacturing processes to understand process features from which defects may occur, and thus may help to explain the mechanistic causation for forging cracking in the future.

5. Conclusions

A UK aerospace fastener manufacturer provided sections of raw material from larger coils, with different observed behavior during axial forging processes to produce the fastener pins. These samples were characterized by their microstructural properties and their mechanical properties. This was to attempt to understand fundamental differences in the supplied raw material bar, which may give rise to this different through-process behavior. The following conclusions are drawn.

- Material that has good forgeability has a slightly higher β-phase volume fraction than poor forgeability material. Recalling that oxygen and other trace elements can be a significant α stabilizer, it is possible that minor element chemical composition variation, whilst within specification, produces a small variation in α phase volume fraction in material, through the manufacturing route.
- Bar material that behaves best during axial forging retains a softer core region, with slightly higher β-phase volume fraction in the core than the outer radius. The core has Vickers hardness values up to 30 Hv lower than the harder outer radius region. This more malleable core, which remains hotter than the chilling edges, promotes plastic deformation at the central region, to allow the pin to fill the forging recess more easily.
- The bar manufacturing process will induce a compressive residual stress field in the outer radius region, which is known to further increase hardness and yield strength. Bars of smaller diameter have likely been drawn to greater reduction of diameter, propagating the high compressive residual stresses deeper into the bar, and eventually hardening the softer core.
- The presence of porous micro-voids actually seems to reduce the forgeability of material, especially close-surface voids, which have the potential to act as stress concentrators or crack initiation sites. This is exacerbated for voids with large aspect ratio, or voids that are approximately at the same depth into the surface as their pore diameter.
- Overall, only small differences between material with good forgeability and poor performance is seen. Most likely it is combinations of effects – such as different composition, material properties, strain rate and sample diameter - that determines the susceptibility to form defects during forging. This can only be established for certain using a much larger study than the present one. The present work demonstrates that establishing root causes for non-conformity in highly optimized production processes requires multi factor analysis on sufficiently large data sets.

Acknowledgments

The authors would like to offer thanks to Lisi Aerospace of Rugby, United Kingdom, for the work performed at the company to make this research possible. Additionally, thanks are offered to microscopy and mechanical testing staff at the School of Metallurgy & Materials, University of Birmingham, in particular Dr Mary Taylor, Dr Chris Cooper and Dr Hao Wu, for their support with various activities within the current work. Thanks to Dr Sam Cruchley, Head of Education at the School of Metallurgy & Materials, for facilitating this research project.

Conflict of interest

The authors declare no conflict of interest.

References

[1] Zipay, J.J., Modlin Jr, C.T., Larsen, C.E., The ultimate factor of safety for aircraft and spacecraft – Its history, applications and misconceptions, NASA Public document, https://ntrs.nasa.gov/api/citations/20150003482/downloads/20150003482.pdf
[2] Roy, A., Working paper on the development of aviation Safety margin for aeronautical services, 2013, International Civil Aviation Organization - Aeronautical communications panel (ACP) ACP-WG-F29/WP-09
[3] Boyer, R.; Cotton, J.; Mohaghegh, M.; Schafrik, R. Materials considerations for aerospace applications. *MRS Bull.* **2015**, *40*, 1055–1066, https://doi.org/10.1557/mrs.2015.278.
[4] Melhem G.N., Bandyopadhyay S, Sorrell C.C., Use of aerospace fasteners in mechanical and structural applications, Ann. J. Materials Sci Eng., 2014; 1(4): 5.
[5] Centrich, X.T.; Shehab, E.; Sydor, P.; Mackley, T.; John, P.; Harrison, A. An Aerospace Requirements Setting Model to Improve System Design. *Procedia CIRP* **2014**, *22*, 287–292, https://doi.org/10.1016/j.procir.2014.07.127.
[6] Owen, B.; Lee, D.S.; Lim, L. Flying into the Future: Aviation Emissions Scenarios to 2050. *Environ. Sci. Technol.* **2010**, *44*, 2255–2260, https://doi.org/10.1021/es902530z.

[7] Reeves P., Example of econolyst research—Understanding the benefits of AM on CO2. Econolyst Ltd. 2012.
[8] Williams, J.C.; Boyer, R.R. Opportunities and Issues in the Application of Titanium Alloys for Aerospace Components. *Metals* **2020**, *10*, 705, https://doi.org/10.3390/met10060705.
[9] Shunmugavel, M.; Polishetty, A.; Littlefair, G. Microstructure and Mechanical Properties of Wrought and Additive Manufactured Ti-6Al-4V Cylindrical Bars. *Procedia Technol.* **2015**, *20*, 231–236, https://doi.org/10.1016/j.protcy.2015.07.037.
[10] Wu, H., Subramanian, G., University of Birmingham internal report, 2022.
[11] Fan, Y.; Tian, W.; Guo, Y.; Sun, Z.; Xu, J. Relationships among the Microstructure, Mechanical Properties, and Fatigue Behavior in Thin Ti6Al4V. *Adv. Mater. Sci. Eng.* **2016**, *2016*, 1–9, https://doi.org/10.1155/2016/7278267.
[12] Luo, J.; Li, M.; Yu, W.; Li, H. The variation of strain rate sensitivity exponent and strain hardening exponent in isothermal compression of Ti–6Al–4V alloy. *Mater. Des.* **2010**, *31*, 741–748, https://doi.org/10.1016/j.matdes.2009.09.055.
[13] Hu, J.; Mu, Y.; Xu, Q.; Yao, N.; Li, S.; Lei, X. The Effect of the Forging Process on the Microstructure and Mechanical Properties of a New Low-Cost Ti-5Al-1.5Mo-1.8Fe Alloy. *Materials* **2023**, *16*, 5109, https://doi.org/10.3390/ma16145109.
[14] Zhang, Z.; Wang, T.; Lin, P. Effect of forging steps on microstructure evolution and mechanical properties of Ti-6Al-4V alloy during multidirectional isothermal forging. *Procedia Manuf.* **2020**, *50*, 817–821, https://doi.org/10.1016/j.promfg.2020.08.147.
[15] Campanella, D.; Buffa, G.; El Hassanin, A.; Squillace, A.; Gagliardi, F.; Filice, L.; Fratini, L. Mechanical and microstructural characterization of titanium gr.5 parts produced by different manufacturing routes. *Int. J. Adv. Manuf. Technol.* **2022**, *122*, 741–759, https://doi.org/10.1007/s00170-022-09876-9.
[16] Fang, X.; Yang, J.; Liu, L.; Wang, Z. Fatigue life prediction model of Ti-6Al-4V alloy forgings based on forging process parameters. *J. Mech. Sci. Technol.* **2022**, *36*, 3341–3352, https://doi.org/10.1007/s12206-022-0613-9.
[17] Alimov, A.; Sizova, I.; Biba, N.; Bambach, M. Prediction of Mechanical Properties of Ti-6Al-4V Forgings Based on Simulation of Microstructure Evolution. *Procedia Manuf.* **2020**, *47*, 1468–1475, https://doi.org/10.1016/j.promfg.2020.04.326.
[18] Rajesh, K.V.D.; Buddi, T.; Mishra, H. FINITE ELEMENT SIMULATION OF Ti-6Al-4V BILLET ON OPEN DIE FORGING PROCESS UNDER DIFFERENT TEMPERATURES USING DEFORM-3D. *Adv. Mater. Process. Technol.* **2021**, *8*, 1963–1972, https://doi.org/10.1080/2374068x.2021.1878708.
[19] Gudas, C. The Effects of Fatigue Cracks on Fastener Loads during Cyclic Loading and on the Stresses Used for Crack Growth Analysis in Classical Linear Elastic Fracture Mechanics Approaches. *Mater. Sci. Appl.* **2020**, *11*, 505–551, https://doi.org/10.4236/msa.2020.117035.
[20] Polmear, I., The light alloys – 5th Ed. Edward Arnold Publishers, New York, USA, 2017
[21] Kopec, M.; Wang, K.; Politis, D.J.; Wang, Y.; Wang, L.; Lin, J. Formability and microstructure evolution mechanisms of Ti6Al4V alloy during a novel hot stamping process. *Mater. Sci. Eng. A* **2018**, *719*, 72–81, https://doi.org/10.1016/j.msea.2018.02.038.
[22] da Rocha, S.S.; Adabo, G.L.; Henriques, G.E.P.; Nóbilo, M.A.d.A. Vickers hardness of cast commercially pure titanium and Ti-6Al-4V alloy submitted to heat treatments. *Braz. Dent. J.* **2006**, *17*, 126–129, https://doi.org/10.1590/s0103-64402006000200008.
[23] ATI Technical datasheet – Ti-6Al-4V (Grade 5), Allegheny Technologies Inc, www.atimaterials.com
[24] Wang, W.; Xu, X.; Ma, R.; Xu, G.; Liu, W.; Xing, F. The Influence of Heat Treatment Temperature on Microstructures and Mechanical Properties of Titanium Alloy Fabricated by Laser Melting Deposition. *Materials* **2020**, *13*, 4087, https://doi.org/10.3390/ma13184087.
[25] Dmitriy, D. Analysis of residual stress in circular cross-section wires after drawing process. *Procedia Manuf.* **2019**, *37*, 335–340, https://doi.org/10.1016/j.promfg.2019.12.056.
[26] Tang, B.; Wang, Q.; Guo, N.; Li, X.; Wang, Q.; Ghiotti, A.; Bruschi, S.; Luo, Z. Modeling anisotropic ductile fracture behavior of Ti-6Al-4V titanium alloy for sheet forming applications at room temperature. *Int. J. Solids Struct.* **2020**, *207*, 178–195, https://doi.org/10.1016/j.ijsolstr.2020.10.011.
[27] Tammas-Williams, S.; Withers, P.J.; Todd, I.; Prangnell, P.B. The Influence of Porosity on Fatigue Crack Initiation in Additively Manufactured Titanium Components. *Sci. Rep.* **2017**, *7*, 1–13, https://doi.org/10.1038/s41598-017-06504-5.
[28] Tosha. K., Influence of residual stresses on the hardness number in the affected layer produced by shot peening, 2nd Asia-Pacific Forum Precision Surface Finishing and Deburring Technology, Seoul, Korea, 2002.
[29] Rudnytskyj, A.; Varga, M.; Krenn, S.; Vorlaufer, G.; Leimhofer, J.; Jech, M.; Gachot, C. Investigating the relationship of hardness and flow stress in metal forming. *Int. J. Mech. Sci.* **2022**, *232*, https://doi.org/10.1016/j.ijmecsci.2022.107571.

[30] Venkatesh, B.; Chen, D.; Bhole, S. Effect of heat treatment on mechanical properties of Ti–6Al–4V ELI alloy. *Mater. Sci. Eng. A* **2009**, *506*, 117–124, https://doi.org/10.1016/j.msea.2008.11.018.
[31] Zhao, Q.; Sun, Q.; Xin, S.; Chen, Y.; Wu, C.; Wang, H.; Xu, J.; Wan, M.; Zeng, W.; Zhao, Y. High-strength titanium alloys for aerospace engineering applications: A review on melting-forging process. *Mater. Sci. Eng. A* **2022**, *845*, https://doi.org/10.1016/j.msea.2022.143260.